Cationic Solution and Solid-State Emitters – Robust Imaging Agents for Cells, Bacteria, and Protists

Justin Dubbert+,[a] Alexander Höing+,[d] Nadine Graupner,[c] Ľubomír Rajter,[c] Micah Dunthorn,[f] Shirley K. Knauer,[d] Anzhela Galstyan,[e] Fabio Rizzo,[b, g] and Jens Voskuhl*[a]

Abstract: A library of eight different cationic emitters with emission properties in solution and in solid-state (solution and solid-state emitters – SSSE) is presented. These compounds, bearing either ammonium or pyridinium groups, have been investigated regarding their photophysical properties as well as their potential application in biological imaging. Besides high quantum yields as well as a high degree of stability during the imaging process, it was additionally revealed that a broad range of biological targets can be addressed, such as different bacterial strains, human cells as well as protists. The reported SSSE approach employing the mentioned robust emitters for biological imaging, will contribute to a rapid and facile way to design and apply affordable emitters with outstanding properties. Additionally, these emitters will overcome the drawbacks of classical luminophores and agents featuring well-known aggregation-induced emission (AIE) or aggregation-caused quenching (ACQ) properties.

Introduction

Compounds capable of emitting light from their excited state are commonly referred to as luminophores, without distinguishing between the excited states from which the emission occurs.[1] These states can be either singlet or triplet states, leading to fluorescence[2] or phosphorescence,[3] respectively. Besides the emitting states, the degree of aggregation is also known to drastically affect the emission properties.[4] Classical luminophores are known to show quenching of the emission upon molecular aggregation, in the solid-state or at high concentrations due to the formation of "aromatic" stacks favoring non-radiative decay pathways[5], but are able to emit when dissolved in solution. On the other hand, there are compounds behaving contrary to classical emitters featuring emission in the solid and aggregated state[6] or when bound to a specific target.[7] The latter is based solely on the hindrance of motion, leading to a blocking (or reduction) of non-radiative decay processes induced for example, by rotation and vibration.[8] Both phenomena are well known[6a,9] and have been utilized for biomedical applications.[10] Luminophores increasing their emission intensity upon binding have been exploited in DNA and RNA imaging taking advantage of the effect of intercalation and thus motion hindrance.[7a,10a, 11]

It is worth noting that compounds emitting in the solid, aggregated, or bound state have been classified by more recent studies under the term "aggregation-induced emission – AIE", which is somewhat misleading, since not only aggregates but

[a] J. Dubbert,+ Prof. Dr. J. Voskuhl
Faculty of Chemistry (Organic Chemistry)
Center of Medical Biotechnology (ZMB) and
Center for NanoIntegration (CENIDE)
University of Duisburg-Essen
Universitätsstrasse 7, 45117 Essen (Germany)
E-mail: jens.voskuhl@uni-due.de

[b] Dr. F. Rizzo
Center for Soft Nanoscience (SoN)
Westfälische Wilhelms-Universität Münster
Busso-Peus-Str. 10, 48149 Münster (Germany)

[c] Dr. N. Graupner, Dr. Ľ. Rajter
Faculty of Biology, Eukaryotic Microbiology, Phycology
University of Duisburg-Essen
Universitätsstrasse 5, 45141 Essen (Germany)

[d] Dr. A. Höing,+ Prof. Dr. S. K. Knauer
Institute for Molecular Biology II
Center for Medical Biotechnology (ZMB)
University of Duisburg-Essen
Universitätsstrasse 5, 45117 Essen (Germany)

[e] Prof. Dr. A. Galstyan
Faculty of Chemistry (Analytical Chemistry)
Center for NanoIntegration (CENIDE) and
Center for Water and Environment Research (ZWU)
University of Duisburg-Essen
Universitätsstrasse 5, 45117 Essen (Germany)

[f] Prof. Dr. M. Dunthorn
Natural History Museum
University of Oslo, N-0318, Oslo (Norway)

[g] Dr. F. Rizzo
Institute of Chemical Science and Technologies "G. Natta" (SCITEC)
National Research Council (CNR)
Via G. Fantoli 16/15, 20138 Milan (Italy).

[+] These authors contributed equally to this manuscript.

📃 Supporting information for this article is available on the WWW under https://doi.org/10.1002/chem.202300334

also monomers reveal emission enhancement when entrapped in a sterically demanding environment. These compounds have been used to stain, recognize and investigate proteins,[12] small molecules[13] and cells[14] as well as specific cellular organelles.[10c,d] A rather prominent class of compounds combining both benefits of classical and AIE luminophores has been investigated over the past decade. These compounds are denoted as dual-state emitters (DSE) featuring emission properties in solution and the solid/aggregated state with nearly equal quantum yields.[4b,15] To avoid confusion, we prefer to use the term solution and solid-state emitters (SSSE)[16] for this class of molecules, since "dual-state" typically implies emission from different electronic states (e. g. singlet and triplet).[17] Until now, only a limited number of studies utilizing the strength of SSSE have been published in the field of bioimaging. Recently, Wang et al. synthesized donor-acceptor (D-A) type SSSE based on triphenylamine and 1,8-naphthalimide, which have been used for bioimaging at low concentrations.[18] These compounds featured nearly equally high luminescence quantum yield as crystal and in solution. The same group introduced 1,8-naphtholactam as backbone, fabricating solution and solid-state luminophores for lysosomal imaging in a follow-up study.[19] Chou et al. reported in 2019 that dihydrodibenzo[ac]phenazines, in which one of the nitrogens is replaced by either oxygen, sulfur, selenium or carbon reveal striking emission properties in solution due to photoinduced structural planarization (PISP), featuring large Stokes shifts. In the solid state, emission with only marginal Stokes shifts is reported due to a lack of PISP leading to emission from the bent structure.[20]

Previous studies reported by us[16b] and Feng et al.[21] focused on constructing the core motif of SSSE without any further functionalization, showed that the photophysical properties are heavily dependent on the type and position of the chalcogens. This allowed us a relative quickly and easily fine tuning of the emission properties.

Aiming to further expand the field of solution and solid-state emitters suitable for bioimaging, in this contribution we report the synthesis and application of cationic SSSE based on bridged oxo-and thioethers as versatile imaging agents for different biological targets, such as different bacterial strains, human cells, and protists. The presented dyes are bearing two different cationic groups, i. e., ammonium and pyridinium salts, in order to investigate their behavior during the uptake in different biological environments as well as their photophysical properties.

Results and Discussion

A library of eight different cationic solution and solid-state emitters was synthesized and investigated as potential imaging agents for human cells, bacteria, and protists (Figure 1). The syntheses were carried out starting from tetrachloroterephthalonitrile, which was coupled solely to an equivalent of Boc-protected dopamine (**A**)[22] under basic conditions (see Supporting Information). The obtained intermediate (**B**) was reacted
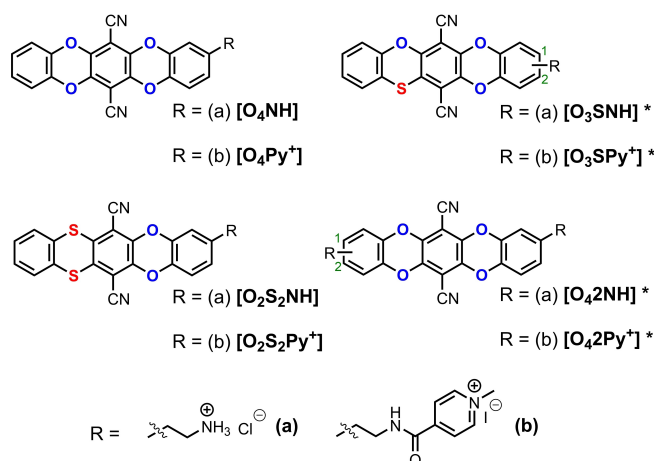

Figure 1. A) Molecular structures of the investigated cationic emitters. *compounds were obtained as a mixture of two inseparable regioisomers at positions 1 and 2. For further information see electronic Supporting Information.

with either catechol, 2-hydroxythiophenol or 1,2-benzenedithiol yielding the compounds O₄NH, O₃SNH and O₂S₂NH after acidic deprotection with hydrochloric acid. The disubstituted compound O₄2NH was directly synthesized by reacting tetrachloroterephthalonitrile with an excess of the dopamine intermediate (**B**) followed by the same deprotection (see Supporting Information).

These four compounds were then converted into the pyridinium derivatives using isonicotinic acid under peptide coupling conditions followed by quaternization with methyl iodide. The compounds O₄Py⁺, O₃SPy⁺, O₂S₂Py⁺ as well as the dimeric species O₄2Py⁺ were obtained in good yields (see Supporting Information).

It is noteworthy that the four compounds O₃SPy⁺, O₃SNH, O₄2Py⁺ and O₄2NH were obtained as a mixture of two inseparable isomers bearing the functional groups at either position 1 or 2 (Figure 1), as a consequence of the synthetic approach used (for further information see Supporting Information). The photophysical properties of the eight dyes were studied both in solution as well as in the solid-state (Supporting Information Figures S21–S25).

Figure 2 shows the eight compounds either dissolved in dimethyl sulfoxide (DMSO) or in the solid-state. The ammonium compounds exhibit bright emission in solution and in the solid-state ranging from turquoise to yellow depending on the sulfur content, as previously reported.[16b,d] Surprisingly, the four pyridinium compounds showed a different behavior.

Dissolved in DMSO, the pyridinium dyes exhibit a bright emission similar to the ammonium compounds, whereas in the solid-state only the sulfur-containing compounds revealed a weak but well detectable emission (Figure 2 and Table 1).

By comparing the emission maxima in solution and in the solid-state (see Figure 2 and Table 1), we observed that O₄NH, O₃SNH and O₃SPy⁺ exhibit minor changes in the maximum of the emission band, whereas the presence of two lateral arms (O₄2NH) and the high sulfur content (O₂S₂NH and O₂S₂Py⁺)
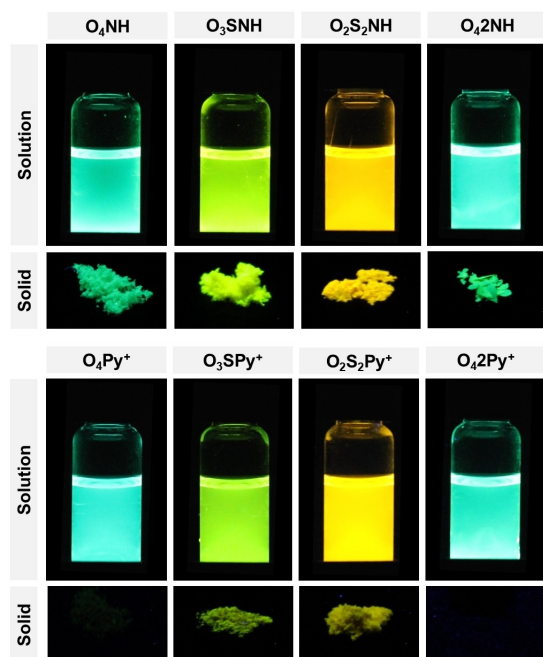
Figure 2. Photographs of the solid and molecularly dissolved (DMSO) compounds under UV-light excitation ($\lambda = 365$ nm).

significantly affect the emission wavelengths (Figures S22 and S23) in both states. To gain a deeper insight into the characteristics of the investigated compounds, we measured photoluminescence quantum yields (Φ_F) and emission lifetimes (τ) in both states (Table 1).

The pure oxygen-containing compound **O$_4$NH** showed the highest Φ_F in solution with a value of 52%. In comparison, the presence of two lateral chains in **O$_4$2NH** does not affect the emission wavelength, while Φ_F decreases to 19%.

An increasing content of sulfur leads to a bathochromic shift in solution, which can be justified by the lower electronegativity and higher π-polarizability of sulfur, accompanied by a decrease in Φ_F.

Furthermore, the presence of two sulfur atoms in the same ring (**O$_2$S$_2$NH** and **O$_2$S$_2$Py$^+$**) should result in a bend in the three-dimensional structure and a drastic deviation from planarity,

resulting in a decreased conjugation length compared to the pure oxygen derivatives.[16d]

The effect for the compounds containing only one sulfur should be considered as an intermediate case featuring a minor distortion in the ring structure containing sulfur and oxygen, which has been previously described for similar ring systems with bonding angles of around 100° for sulfur and 120° for oxygen.[16b,23] Obviously, this intermediate molecular structure also affects the emission wavelength as well as the Φ_F. Very interestingly, the high sulfur content in **O$_2$S$_2$NH** increases the lifetime in the solid-state up to 336 μs, indicating phosphorescence as the radiative mechanism, which is in agreement with our previous study (Figure S25).[16d] This behavior is not preserved in the analogous pyridinium derivative **O$_2$S$_2$Py$^+$**, probably due to the presence of iodine, which acts as a quencher of the intersystem crossing process between the singlet and triplet state.

As known from literature, the heavy atom effect promotes non-radiative decay pathways. Here, iodide as counter-ion influences drastically the photophysical performance of the corresponding derivatives by accelerating non-radiative relaxation.[24] However, in solution, the pyridinium compounds exist as solvent-separated ion pairs, which disables the quenching effect of I$^-$.[25]

On the contrary, in the condensed phase the closely interacting ion pairs annihilate the excitons and lead to a drastic loss of emission in the solid-state.[26] In our case, the deviation from planarity arising from the introduction of sulfur decreases potential quenching processes, leading to a weak but detectable solid-state emission for **O$_2$S$_2$Py$^+$** and **OS$_3$Py$^+$**.

The simple variations of the position and type of chalcogen atoms result in distinct structural differences (planar (**O$_4$**) – distorted (**O$_3$S**) – bent (**O$_2$S$_2$**)) and in a peculiar tuning of the emission color (turquoise (**O$_4$**) – green (**O$_3$S**) – yellow (**O$_2$S$_2$**)). This unique performance might allow a wide range of possible biomedical applications and the adoption for a plethora of imaging purposes. To validate this hypothesis, we set out to thoroughly investigate the compounds' effects on cell viability, their cellular uptake, and intracellular localization in a human tumor cell line (HeLa).

To first assess potential toxic effects, HeLa cells were incubated in compound-supplied medium for 24 h, and cell viability was determined by an MTS assay. Notably, all

Table 1. Photophysical properties of all investigated compounds in solution (DMSO) and in solid-state at rt.

| Compound | Solution state[b] | | | | Solid-state | | | |
	λ_{abs} [nm]/ε [cm^{-1} M^{-1}][a]	λ_{em} [nm][a]	τ [ns]	Φ_F [%][c]	λ_{ex} [nm][e]	λ_{em} [nm]	τ_{av}	Φ_F [%][c]
O$_4$NH	430/9450	494	5.73	52	~410	500	0.66 ns[d]	24
O$_3$SNH	430/5900	542	6.60	46	~410	544	2.70 ns[d]	26
O$_2$S$_2$NH	417/4490	581	4.84	20	~420	592	336.26 μs[d]	16
O$_4$2NH	431/4530	497	3.95[d]	19	~410	529	1.97 ns[d]	13
O$_4$Py$^+$	431/5175	492	3.06	20	–	–	–	–
O$_3$SPy$^+$	432/4225	538	5.06	35	~420	538	2.67 ns[d]	1
O$_2$S$_2$Py$^+$	418/5790	584	4.12	18	~420	566	2.03 ns[d]	6
O$_4$2Py$^+$	433/7380	493	2.61	22	–	–	–	–

[a] most bathochromically shifted maximum. [b] in DMSO, $c \approx 20$ μM. [c] quantum yields were determined using an integrated sphere (absolute method). [d] biexponential decay. [e] average excitation wavelength due to the large excitation band.

Chemistry–A European Journal

Research Article
doi.org/10.1002/chem.202300334

Chemistry Europe
European Chemical
Societies Publishing

ammonium compounds revealed cellular toxicity at low micromolar concentrations. In contrast we observed no or neglectable effects on cell viability for the pyridinium compounds (see Figures S44 and S45). Afterwards, cells were treated with the cell stain Cell Tracker™ and incubated in compound-supplied medium for 1 h.

Uptake and localization were analyzed by confocal laser scanning microscopy (CLSM). To definitely confirm the internalization, we also generated 3D images from image stacks, which allowed a tomographic assessment of the compounds' intracellular localization (see Figures S36–S43), which has been used as a versatile method beforehand.[27] Although all ammonium compounds were internalized by the cells, in particular **O₄NH**, **O₃SNH** and **O₂S₂NH** accumulated in cytoplasmic vesicular structures or aggregates (Figure 3, and Figures S26–S28). We were surprised to find that the dimeric compound **O₄2NH** revealed a completely different distribution pattern. Most strikingly, this emitter was not distributed homogeniously in the cytoplasm, but was also present in the nucleus accumulating at the nucleoli, which could be identified in the phase contrast images (see Figure S29). Futhermore, the compound accumulated in a structure surrounding the nucleus, which resembles the endoplasmic reticulum (Figure 3 and see Figure S29).

The pyridinium compounds were also internalized by the cells and revealed a more homogeneous cytoplasmic distribution (Figure 3 and see Figures S30-S33). None of them was present in the nucleus, but they all showed local accumulations surrounding the nucleus similar to **O₄2NH**. Noteworthy, these areas overlap with the ones enriched with Cell Tracker™. We therefore experimentally excluded the unlikely, but potential possibility of cross-talk or artefacts (see Figures S34 and S35).

Considering the essential role of bacteria in the ecosystem and in health, their staining is of great importance for the detection and understanding of their interactions with the external environment.[28] The success of a particular staining procedure depends largely on the chemical properties of the fluorescent probes, whereby fine-tuning of the structure allows the imaging agent to be matched to the available excitation source and the employed bacterial species. To demonstrate the application potential of our emitters for bacterial imaging, first viability studies were performed using the Alamar Blue™ assay.[29] The benefits of this assay compared to other redox indicators include its low toxicity and the fact that its reduced form is soluble in aqueous media, making it practical to perform serial measurements from the same plate. For these experiments, *B. subtilis* DB 104 was used as a model for Gram-positive bacteria and *E. coli* Nissle 1917 as a Gram-negative bacterial strain. At a concentration of 10 μM, only the compounds containing two positive charges (**O₄2NH** and **O₄2Py⁺**) exhibited toxicity against both strains, whereas the activity of **O₄2Py⁺** against *E-coli* was moderate (ca. 40% reduction of viability) (Figure S46). Basically, all our compounds harbor hydrophobic domains as well as cationic charges linked by short alkyl chains. Moreover, they are characterized by a suitable topology and size to interact with lipid membranes of bacteria. However, due to the negative membrane potential of bacteria, the interaction of dyes with two positive charges is stronger, presumably leading to membrane rupture.[30] As expected, Gram-negative bacteria are less sensitive to membrane damage than Gram-positive strains due to their more complex membrane composition, which together with the altered lipophilicity of **O₄2Py⁺**, explains its lower activity against Gram-negative *E. coli* (Figure S46).[31]

We further analyzed the staining ability of the compounds by incubation of the bacteria for 1 h with 10 μM solutions of the corresponding emitters. Stained samples were imaged by fluorescence microscopy (Figure 4, and see Supporting Information Figures S47–S50). The interior of the cells was stained with the nucleic acid dye Hoechst 33342. Notably, all our charged
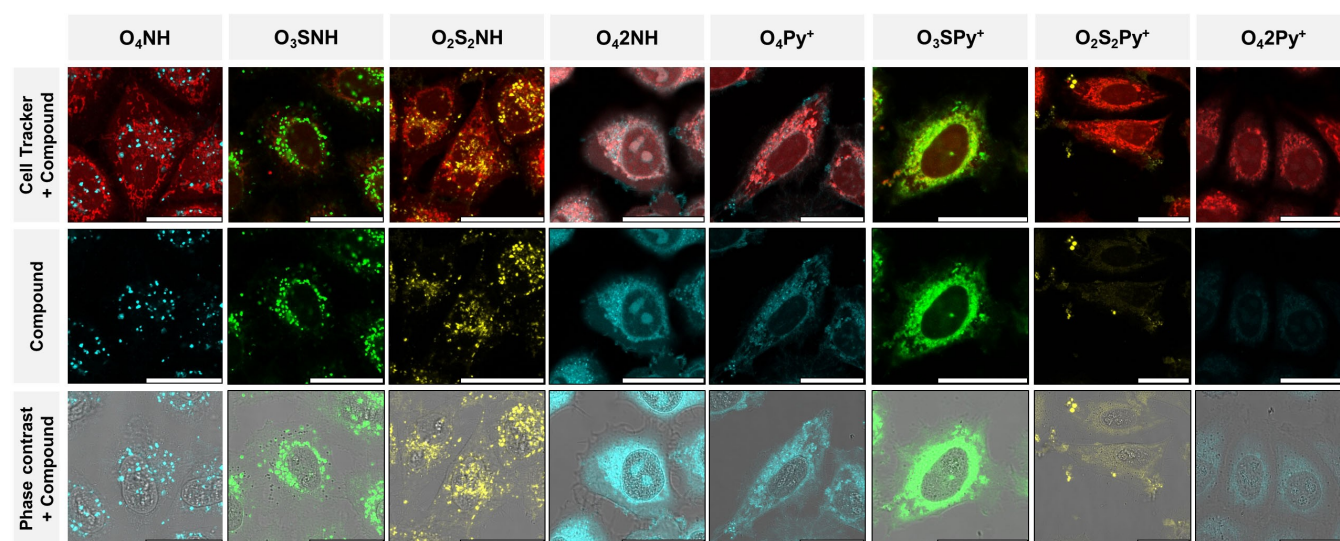

Figure 3. Confocal laser scanning microscopy of HeLa cells incubated with a concentration of 30 μM of the indicated compounds and a cytoplasmic stain (Cell Tracker™ (red)). The scale bar represents 30 μm. Colors of the compounds were adjusted according to the emission wavelengths of the compounds used.
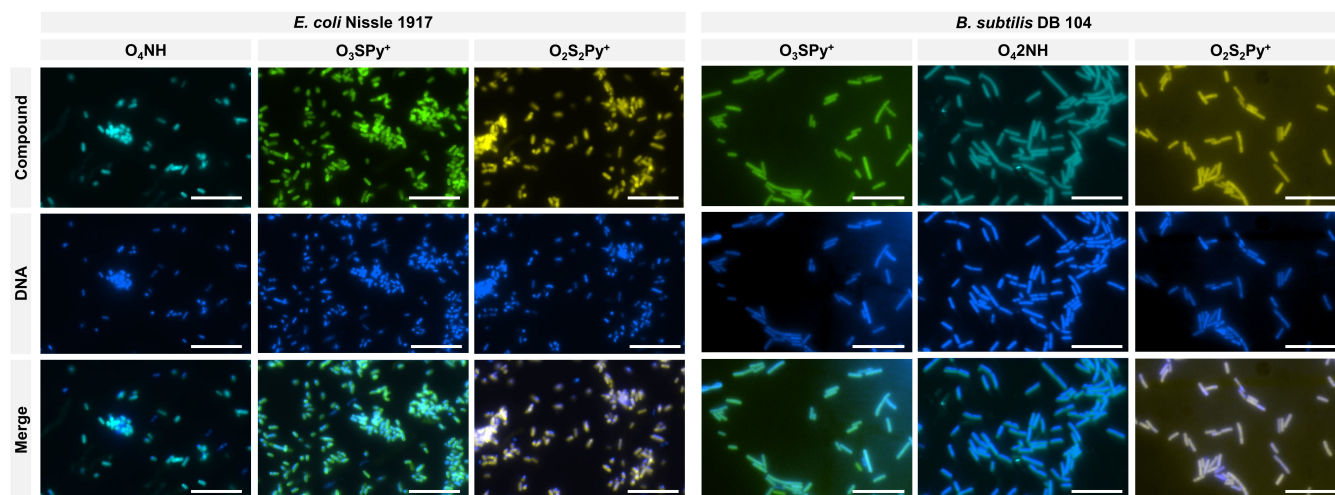
Chemistry–A European Journal

Research Article
doi.org/10.1002/chem.202300334

Chemistry Europe
European Chemical
Societies Publishing

Figure 4. Fluorescence microscopy images of selected compounds after incubation of different bacterial strains for 1 h with a compound concentration of 10 µM. The scale bar represents 10 µm. The colors of the compounds O_4NH, O_3SPy^+, $O_2S_2Py^+$ and O_42NH were adjusted afterwards according to the emission wavelengths.

emitters are indeed homogeneously distributed, and thus can be applied for bacterial imaging, whereas only the single armed cationic emitters do not alter the viability (Figure 4).

In addition to different bacterial strains and human tumor cells, we tested the three ammonium derivatives, namely O_4NH, O_3SNH and O_2S_2NH, on *Paramecium tetraurelia*, a genus of eukaryotic, unicellular ciliates. These three compounds were selected since they featured the highest Φ_F in solution and in the solid-state and were easily synthetically available. In total, four different parameters were screened – concentration, effects of fixation, which helps to visualize the motile *Paramecium tetraurelia*, temperature and incubation time (a selection of different images at varying parameters is shown in Figure 5, for an overview of all screened parameters, see Figure S51–S58). As expected, the concentration of the compound was the most critical parameter for a successful visualization. Reliable results were obtained with a concentration of 100 µM and an incubation time of 1 h, resulting in a high contrast and only minor background staining as revealed by fluorescence microscopy (Chapter 6 in the Supporting Information. Therefore, we used this concentration in all further experiments with *Paramecium tetraurelia*, Figures S51–S58). To our surprise, the incubation time did not significantly affect uptake and contrast, nor did the choice of fixative and changes in the incubation temperature (see Figures S51–57). Importantly, our stains were not lethal to *Paramecium tetraurelia*, as demonstrated by the observation of the living cells without fixative (Figure S53 and S56).

For all three analyzed compounds, efficient co-localization with *Paramecium tetraurelia* was observed, resulting in well-detectable emission signals of O_4NH, O_3SNH or O_2S_2NH. As shown in Figure 5, the cationic luminophores stain the entire organism and accumulate in the inner vacuoles, such as food vacuoles and the cytoplasm. Interestingly, the finely structured cilia can also be easily visualized using O_4NH (Figure S58). To
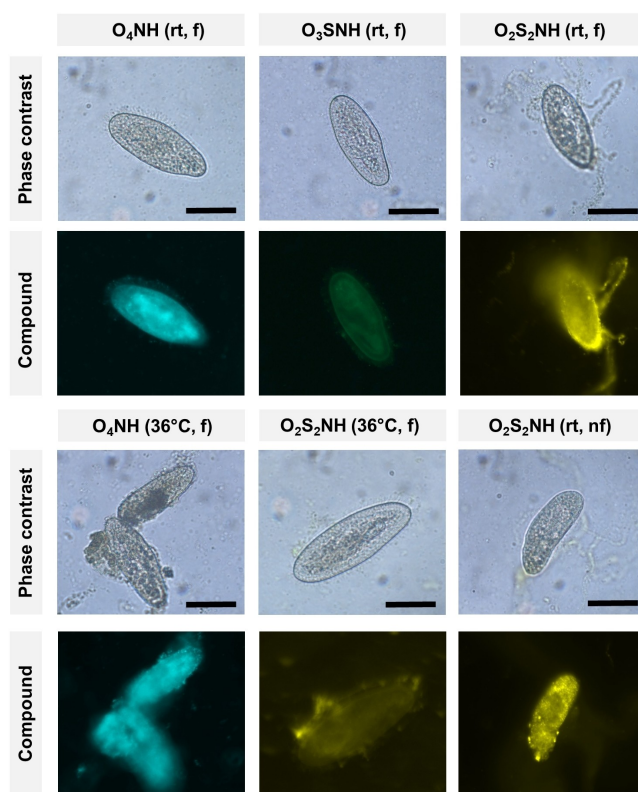

Figure 5. Fluorescence microscopy and phase contrast images of *Paramecium tetraurelia* incubated with O_4NH, O_3SNH, and O_2S_2NH for 1 h ($c = 100$ µM). rt = room temperature, f = fixation, nf = no fixation. The scale bar represents 50 µm. Colors of the compounds were adjusted according to the emission wavelengths of the compounds used.

summarize, the used luminophores can visualize some taxonomically essential characteristics such as vacuoles, nuclei, and cilia, which is a key factor in species identification.

Chemistry–A European Journal

Research Article
doi.org/10.1002/chem.202300334

Chemistry
Europe
European Chemical
Societies Publishing

Since effective, universal, and easy-to-use stains for protists are still rarely described in biodiversity and ecological studies, we believe that this simple class of compounds can open new avenues for reliable visualization of protists and their diagnostic features.

Conclusion

In this contribution we developed emissive cationic solution and solid-state emitters (SSSE) that revealed striking photophysical properties. These eight compounds were synthesized in short synthetic routes with good yields. The majority of the emitters showed only moderate toxicity over a broad range of concentrations, and were therefore evaluated for their applicability as imaging agents. We demonstrated their efficient uptake by several different biological specimens such as human HeLa cells, different bacterial strains as well as the ciliate *Paramecium tetraurelia*, indicating a wide range of applications. Thus, they are characterized as a broadly applicable class of fluorophores suitable to stain different targets such as bacteria, cells, and protists. Future research might involve the selective targeting of specific cell compartments such as mitochondria, nuclei, membranes, lysosomes or endosomes by attachment of compatible and specific recognition units.

Experimental Section

Cell Culturing: Human cervical cancer cells (HeLa Kyoto, RRID: CVCL 1922) were cultivated at 37 °C in a relative humidity of about 95% and 5% CO_2. If not stated otherwise, Dulbeccos modified eagle medium (DMEM) (Thermo Fisher Scientific) was supplied with 10% (v/v) fetal calf serum (FCS) (Life Technologies GmbH), 2 mM L-Glutamine and Antibiotic-Antimycotic (AA) (Life Technologies GmbH). Cells were regularly split at a confluency of about 70%–90% and incubation steps were carried out at 37 °C with 5% CO_2.

Toxicity Assay: HeLa cells were diluted to achieve 10% confluence in 100 µL DMEM and seeded into Corning 96 Well microplates (Sigma-Aldrich) The cells were incubated at 37 °C for 3 h to make them adherent. The medium was removed for DMEM containing the 0.5–30 µM respective compound. Since the compounds were dissolved in DMSO, we added respective DMSO concentrations to the untreated controls for later normalization The cells were then incubated for 24 h. Toxicity was determined using a colorimetric MTS (3-(4,5-dimethylthiazol-2-yl)-5-(3-carboxymethoxyphenyl)-2-(4-sulfophenyl)-2H-tetrazolium) assay according to manufacturer's instructions (*Cell Titer 96 AQueous One*, Promega). In viable cells, MTS is converted to formazan with an absorbance maximum at 490 nm and the quantity is proportional to the number viable cells. The compound-containing medium was removed, cells were washed with PBS once to remove excess compound and 100 µL fresh DMEM was added. 20 µL *Cell Titer AQueous One* (Promega) were added and after 1 h incubation, the absorbance at 490 nm was measured utilizing a plate reader *Promega Glow Max* (Promega). Results were normalized to untreated cells and are the mean of at least three replicates ± standard deviation. Data was fit using a dose-response fit (Origin).

Supporting Information: Full experimental details of the target compounds, photophysical characterisation, selected spectra, and details for the biological imaging, can be found in the Supporting Information. Additional references cited within the Supporting Information.[32–36]

Conflict of Interests

The authors declare no conflict of interest.

Data Availability Statement

The data that support the findings of this study are available in the supplementary material of this article.

Keywords: bacteria · bioimaging · emission · HeLa cells · protists

[1] a) B. M. Krasovitskii, B. M. Bolotin, *Chem. Heterocycl. Compd.* **1974**, *10*, 1269–1284; b) B. Valeur, M. N. Berberan-Santos, *Molecular Fluorescence* (Eds. B. Valeur, M. N. Berberan-Santos). **2012**, Wiley-VCH, Weinheim, Germany, pp. 1–30.

[2] B. Valeur, M. N. Berberan-Santos, *Characteristics of Fluorescence Emission. In Molecular Fluorescence* (Eds. B. Valeur, M. N. Berberan-Santos). **2012**, Wiley-VCH, Weinheim, Germany, pp. 53–74.

[3] a) M. Hayduk, S. Riebe, J. Voskuhl, *Chem. Eur. J* **2018**, *24*, 12221–12230; b) Kenry, C. Chen, B. Liu, *Nat. Commun.* **2019**, *10*, 2111.

[4] a) J. Mei, N. L. Leung, R. T. Kwok, J. W. Lam, B. Z. Tang, *Chem. Rev.* **2015**, *115*, 11718–11940; b) J. L. Belmonte-Vázquez, Y. A. Amador-Sánchez, L. A. Rodríguez-Cortés, B. Rodríguez-Molina, *Chem. Mater.* **2021**, *33*, 7160–7184.

[5] J. B. Birks, *Photophysics of Aromatic Molecules*, Wiley-Interscience, London, **1970**, p 90-93 .

[6] a) F. Würthner, *Angew. Chem. Int. Ed. Engl.* **2020**, *59*, 14192–14196; *Angew. Chem.* **2020**, *132*, 14296–14301; b) Y. Hong, J. W. Lam, B. Z. Tang, *Chem. Commun.* **2009**, 4332–4353.

[7] a) J. Olmsted III, D. R. Kearns, *Biochemistry* **1977**, *16*, 3647–3654; b) S. Xie, A. Y. H. Wong, S. Chen, B. Z. Tang, *Chem. Eur. J.* **2019**, *25*, 5824–5847.

[8] a) Q. Peng, Z. G. Shuai, *Aggregate* **2021**, *2*, e91; b) Y. Tu, Z. Zhao, J. W. Y. Lam, B. Z. Tang, *Natl. Sci. Rev.* **2021**, *8*, nwaa260.

[9] a) G. Oster, Y. Nishijima, *J. Am. Chem. Soc.* **2002**, *78*, 1581–1584; b) T. Förster, G. Hoffmann, *Z. Phys. Chem.* **1971**, *75*, 63–76.

[10] a) H. P. Spielmann, D. E. Wemmer, J. P. Jacobsen, *Biochemistry* **1995**, *34*, 8542–8553; b) J. Nygren, N. Svanvik, M. Kubista, *Biopolymers* **1998**, *46*, 39–51; c) J. J. Qian, D. Wang, S. He in *Aggregation-Induced Emission:*

Chemistry–A European Journal

Research Article
doi.org/10.1002/chem.202300334

Chemistry Europe
European Chemical
Societies Publishing

Fundamentals and Applications, Volumes 1 and 2, (Eds. A.Qin, B. Z. Tang), **2013**, Wiley-VCH, Weinheim, Germany, pp. 209–237; d) L. Huang, L. Dai, *J. Polym. Sci. Part A* **2017**, *55*, 653–659.

[11] A. Banerjee, P. Majumder, S. Sanyal, J. Singh, K. Jana, C. Das, D. Dasgupta, *FEBS Open Bio* **2014**, *4*, 251–259.

[12] a) H. Choi, S. Kim, S. Lee, C. Kim, J. H. Ryu, *ACS Omega* **2018**, *3*, 9276–9281; b) X. Zhao, Y. Gao, J. Wang, Y. Zhan, X. Lu, S. Xu, X. Luo, *Chem. Commun.* **2020**, *56*, 13828–13831.

[13] a) M. Hayduk, S. Riebe, K. Rudolph, S. Schwarze, F. van der Vight, C. G. Daniliuc, G. Jansen, J. Voskuhl, *Isr. J. Chem.* **2018**, *58*, 927–931; b) D. M. Li, Y. S. Zheng, *Chem. Commun.* **2011**, *47*, 10139–10141.

[14] a) S. Riebe, C. Vallet, F. van der Vight, D. Gonzalez-Abradelo, C. Wolper, C. A. Strassert, G. Jansen, S. Knauer, J. Voskuhl, *Chem. Eur. J* **2017**, *23*, 13660–13668; b) J. Stelzer, C. Vallet, A. Sowa, D. Gonzalez-Abradelo, S. Riebe, C. G. Daniliuc, M. Ehlers, C. A. Strassert, S. K. Knauer, J. Voskuhl, *ChemistrySelect* **2018**, *3*, 985–991.

[15] a) Y. Sun, T. Wu, F. Zhang, R. Zhang, M. Wu, Y. Z. Wu, X. Z. Liang, K. P. Guo, J. Li, *Dyes Pigm* **2018**, *149*, 73–81; b) Y. Xu, L. Ren, D. Dang, Y. Zhi, X. Wang, L. Meng, *Chem. Eur. J.* **2018**, *24*, 10383–10389; c) D. K. Singh, K. Jang, J. Kim, J. Lee, I. Kim, *ACS Comb. Sci.* **2019**, *21*, 408–416.

[16] a) S. Thulaseedharan Nair Sailaja, I. Maisuls, J. Kosters, A. Hepp, A. Faust, J. Voskuhl, C. A. Strassert, *Beilstein J. Org .Chem.* **2020**, *16*, 2960–2970; b) S. Riebe, S. Adam, B. Roy, I. Maisuls, C. G. Daniliuc, J. Dubbert, C. A. Strassert, I. Schapiro, J. Voskuhl, *Chem. Asian. J.* **2021**, *16*, 2307–2313; c) A. Huber, J. Dubbert, T. D. Scherz, J. Voskuhl, *Chem. Eur. J.* **2023**, *29*, e202202481; d) J. Dubbert, M. Valtolina, A. Huber, T. D. Scherz, C. Wolper, C. G. Daniliuc, O. Filiba, S. Sen, I. Schapiro, F. Rizzo, J. Voskuhl, *ChemPhotoChem* **2023**, *7*, e202200169.

[17] N. A. Kukhta, M. R. Bryce, *Mater. Horiz.* **2021**, *8*, 33–55.

[18] F. Yu, H. Zhao, Y. Li, G. Xia, H. Wang, *Mater. Chem. Front.* **2022**, *6*, 155–162.

[19] M. M. Tan, Y. Z. Li, W. H. Guo, Y. L. Chen, M. D. Wang, Y. G. Wang, B. Z. Chi, H. Wang, G. M. Xia, H. M. Wang, *Dyes Pigm.* **2022**, *201*, 110243.

[20] Y. Chen, D. G. Chen, Y. A. Chen, C. H. Wu, K. H. Chang, F. Y. Meng, M. C. Chen, J. A. Lin, C. Y. Huang, J. Su, H. Tian, P. T. Chou, *Chem. Eur. J.* **2019**, *25*, 16755–16764.

[21] W. Xi, J. Yu, M. Wei, Q. Qiu, P. Xu, Z. Qian, H. Feng, *Chem. Eur. J.* **2020**, *26*, 3733–3737.

[22] A. Dalpiaz, B. Cacciari, M. Mezzena, M. Strada, S. Scalia, *J. Pharm. Sci.* **2010**, *99*, 4730–4737.

[23] L. K. Hiscock, C. Yao, W. G. Skene, L. N. Dawe, K. E. Maly, *J. Org. Chem.* **2019**, *84*, 15530–15537.

[24] a) T. W. Hudnall, F. P. Gabbai, *Chem. Commun.* **2008**, 4596–4597; b) A. Corma, M. S. Galletero, H. Garcia, E. Palomares, F. Rey, *Chem. Commun.* **2002**, 1100–1101.

[25] Y. Marcus, G. Hefter, *Chem. Rev.* **2006**, *106*, 4585–4621.

[26] N. Zhao, J. W. Lam, H. H. Sung, H. M. Su, I. D. Williams, K. S. Wong, B. Z. Tang, *Chem. Eur. J.* **2014**, *20*, 133–138.

[27] a) J. Dubbert, A. Hoing, N. Riek, S. K. Knauer, J. Voskuhl, *Chem. Commun.* **2020**, *56*, 7653–7656; b) A. Sowa, A. Hoing, U. Dobrindt, S. K. Knauer, A. Galstyan, J. Voskuhl, *Chem. Eur. J.* **2021**, *27*, 14672–14680.

[28] S. A. Yoon, S. Y. Park, Y. Cha, L. Gopala, M. H. Lee, *Front. Chem.* **2021**, *9*, 743923.

[29] A. Galstyan, Y. K. Maurya, H. Zhylitskaya, Y. J. Bae, Y. L. Wu, M. R. Wasielewski, T. Lis, U. Dobrindt, M. Stepien, *Chem. Eur. J.* **2020**, *26*, 8262–8266.

[30] C. Ghosh, J. Haldar, *ChemMedChem* **2015**, *10*, 1606–1624.

[31] J. Sun, S. T. Rutherford, T. J. Silhavy, K. C. Huang, *Nat. Rev. Microbiol.* **2022**, *20*, 236–248.

[32] A. Dalpiaz, B. Cacciari, M. Mezzena, M. Strada, S. Scalia, *J. Pharm. Sci.* **2010**, *99*, 4730–4737.

[33] R. Burger, P. Bigler, *J. Magn. Reson.* **1998**, *135*, 529–534.

[34] N. R. Babij, E. O. McCusker, G. T. Whiteker, B. Canturk, N. Choy, L. C. Creemer, C. V. D. Amicis, N. M. Hewlett, P. L. Johnson, J. A. Knobelsdorf, F. Li, B. A. Lorsbach, B. M. Nugent, S. J. Ryan, M. R. Smith, Q. Yang, *Org. Process Res. Dev.* **2016**, *20*, 661–667.

[35] J. Dubbert, M. Valtolina, A. Huber, T. D. Scherz, C. Wölper, C. G. Daniliuc, O. Filiba, S. Sen, I. Schapiro, F. Rizzo, J. Voskuhl, *ChemPhotoChem* **2023**, *7*, e202200169.

[36] C. A. Schneider, W. S. Rasband, K. W. Eliceiri, *Nat. Methods* **2012**, *9*, 671–675.